

50 db was measured with the *C*-band limiter at 5.65 kMc. The limiter can be expected to have a dynamic range of approximately this value.

Fig. 3 illustrates the low power insertion loss characteristics over a range of frequencies in *C*-band. The biasing field was independently set for resonance at each frequency. The strip-to-strip isolation in the absence of an applied field was in excess of 40 db at each frequency.

Fig. 4 represents the output pulse of the limiter as observed on an oscilloscope. The trailing edge of the limited pulse is seen to extend beyond the trailing edge of the incident pulse. This is due to a "kickback" of energy from the garnet spin system. This effect has been observed to last from about 0.2 to 0.4 μ sec, and should be regarded as the recovery time of the limiter.

The spike leakage characteristics of the limiter are favorable. Fig. 5 is a plot of incident pulse width vs average power out of the limiter at the three *C*-band frequencies. The peak power was held at 2 kw and the

PRF at 500 for each measurement. The intercepts at the vertical axis can be used to calculate the sum of spike leakage energy and kickback energy. The results as shown vary from 0.5 to 0.9 erg. Kickback energy can be estimated from measurements on the oscilloscope to be about 0.2 erg. Spike leakage from the limiter is therefore in the neighborhood of 0.5 erg.

The very low limiting thresholds of the "first-order" crossed-strip limiters reported, presently restrict their useful range to low peak power levels. In contrast with the first-order limiter, the second-order device reported here offers immediate promise for use in the capacity of crystal protection in the medium power range up to about 10-kw peak power.

The authors wish to thank D. E. Tribby and A. C. Setlow for their very competent technical assistance.

J. CLARK

J. BROWN

Applied Physics Section
Sperry Microwave Electronics Co.
Clearwater, Fla.

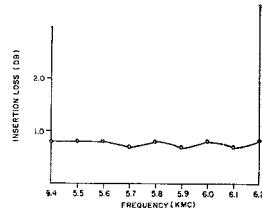


Fig. 3—Low-power (approximately 1-mw) insertion loss characteristics of the *C*-band gyromagnetic coupling limiter.

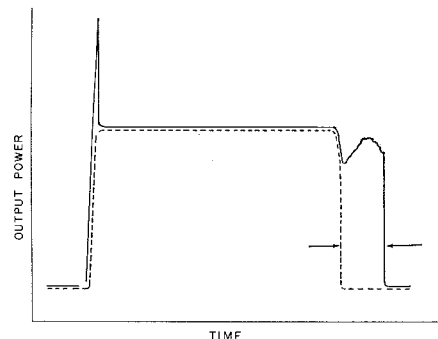


Fig. 4—Wave shape of the limited pulse as observed on the oscilloscope. Dotted line represents incident waveform attenuated for comparison with the limited pulse. The extended portion of the limited pulse is contained between the arrows.

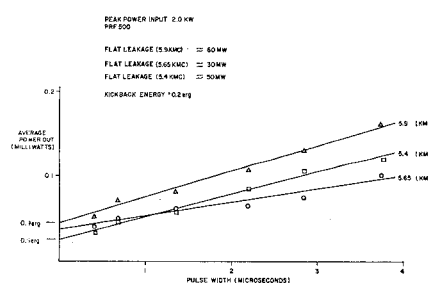


Fig. 5—Average power out of the *C*-band gyromagnetic coupling limiter at varying incident pulse widths.

at 75-kw peak power (0.001 duty cycle) and found to maintain 30 db of isolation with 0.3-db insertion loss.

The amplifier limiter combination was subjected to 1.2-kw peak (0.0015 duty cycle) power input. The power input was increased in small increments from about 25 μ w to 1.2 kw. The amplifier was allowed to run for a few minutes at each new power level and then returned to 25 μ w to check for proper operation. The amplifier showed no adverse characteristics or change in performance as a result of the increases in power.

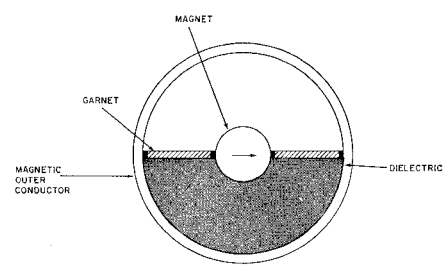


Fig. 1—Coaxial subsidiary resonance limiter.

In the second experiment, a gyromagnetic coupling limiter similar to the one described by DeGrasse² was used to protect a 1N23 crystal. The crystal was mounted directly on the output of the limiter in a tunable coaxial mount.

The tests were carried out at 5.7 kMc. The characteristics of the limiter used are fully described in an accompanying publication.³ As indicated there the power output of the limiter declines after passing through a maximum of approximately 300 mw. The power output decreases as the susceptibility of the YIG sphere declines. The power output will continue to decrease until the limiting level is equal to the isolation between coupling strips in the absence of a resonance biasing field on the sphere. For the configuration used in this test the isolation between strips was 53 db. At some input power level (probably about 10 kw for this configuration) the output power will begin to rise monotonically.

For the actual test the power input to the limiter was raised in steps to 5 kw and the detected waveform of the crystal was monitored. Several crystals were selected at random and tested in this fashion. They all performed essentially the same, and showed no adverse effects. Here again only short-term effects were being tested. Fig. 2 shows a photograph of the waveform of the output of one of the crystals with 1.2 kw incident on the limiter.

In a third experiment, at 5.65 kMc, a waveguide subsidiary resonance limiter was used as a first-stage limiter ahead of the gyromagnetic coupling limiter. The characteristics of the first-stage limiter are shown in Fig. 3. A peak input power of 25 kw was

* Received by the PGMTT, September 18, 1961. This work was supported in part by the U. S. Army Signal Res. and Dev. Lab. under Contract No. DA-36-039-SC-85330, and in part by the U.S.A.F. Rome Air Dev. Ctr. under Contract No. AF30(602)-2296.

¹ J. Clark and J. Brown, "Miniatrized, temperature stable, coaxial *Y*-junction circulators," IRE TRANS. ON MICROWAVE THEORY AND TECHNIQUES (Correspondence), vol. MTT-9, pp. 267-269; May, 1961.

² R. W. DeGrasse, "Low loss gyromagnetic coupling through single crystal garnets," J. Appl. Phys., suppl. to vol. 30, pp. 155s-160s; April, 1959.

³ J. Clark and J. Brown, "Gyromagnetic coupling limiter at *C*-band," this issue, p. 84.

applied to the combination limiter. Fig. 4 shows a photograph of the oscilloscope presentation of a 1N23 detector on the output of the second-stage limiter. The input pulse, attenuated 53 db, is shown for comparison. Measurements indicate that the total spike leakage is 0.2 erg of energy. The maximum power available for this particular test was 25 kw. There were no indications of either diode or limiter failure, and it could be reasonably expected that the combination could withstand higher power.

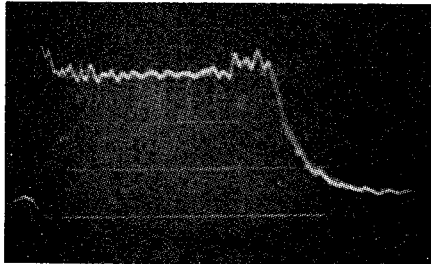


Fig. 2—Direct output of the gyromagnetic coupling limiter through a 1N23 detector. Time base is 0.2 μ sec per square.

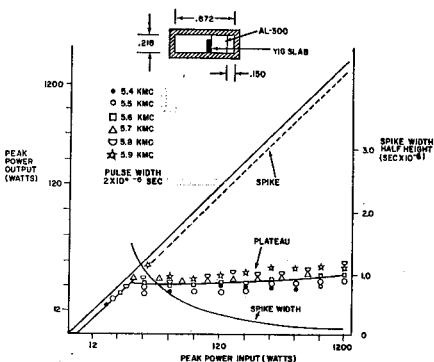


Fig. 3—Characteristics of the subsidiary resonance first-stage limiter.

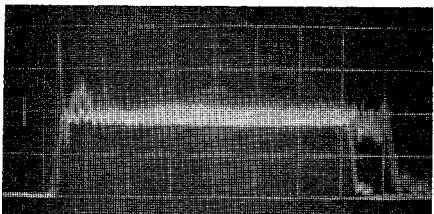


Fig. 4—Direct output of the two-stage limiter through a 1N23 detector. The input attenuated 53 db is shown for comparison. Time base is 0.2 μ sec per square.

In conclusion, it has been shown that receiver protection can be afforded by ferrimagnetic limiters. These limiters are passive, and when used as specified should have no apparent lifetime limitations.

J. BROWN

J. CLARK

Applied Physics Section
Sperry Microwave Electronics Co.
Clearwater, Fla.

Temporal Instabilities in Traveling-Wave Parametric Amplifiers*

The basic traveling-wave parametric amplifier (TWPA) [1]-[3], as here defined, consists of an all-pass uniform transmission-line structure in which the distributed circuit elements are modulated in time and space by a progressive pumping wave. TWPA's, in general, have aroused great interest due to the possibilities of wide-band amplification, as predicted by coupled mode theory [2]-[4]. It is the purpose of this communication to show that temporal instabilities exist on the basic TWPA (or its dual [1]) when the frequency relations are of the negative-resistance type (the inverting modulator of Manley and Rowe [6]). It is found, from the exact solution for time harmonic waves existing on this line, that under these conditions waves growing in time are present, rather than waves growing in distance along the line.

The exact solution for time harmonic waves on the uniform transmission line, which possesses distributed coefficients periodically modulated in time and space (Fig. 1), is [7]

$$V(z, t) = e^{i(\omega t - kz)} \sum_{n=-\infty}^{\infty} V_n e^{i(\omega_1 t - k_1 z)n} \quad (1)$$

where

- ω = angular frequency of the "signal"
- k = propagation wavenumber of the "signal"
- ω_1 = angular frequency of pumping wave (specified)
- k_1 = propagation wavenumber of pumping wave
- $= \omega_1/c'$
- c' = phase velocity of pumping wave (specified).

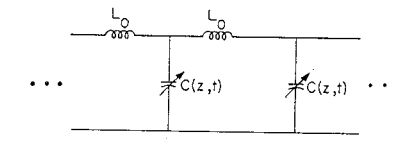


Fig. 1—Basic traveling-wave parametric amplifier.

It may be shown that this solution is a mathematically complete solution and is valid everywhere except [7], [8] where the pump phase velocity (c') is within a specified range near the propagation velocity of the line [$v_{p_0} = (L_0 C_0)^{-1/2}$]. This range has been called the "sonic region" [7], [8], and its width is dependent on the amplitude of modulation, M [7], [8].

The differential equation governing the modulated transmission line is as follows:

$$\frac{\partial^2 V(z, t)}{\partial z^2} = L_0 \frac{\partial^2}{\partial t^2} [C(z, t)V(z, t)]. \quad (2)$$

The substitution of (1) into (2) leads to the following three-term recursion relation [7], [8], [10], [11] for the time-space harmonic amplitudes

$$V_{n+1} + D_n V_n + V_{n-1} = 0, \quad (3)$$

where

$$D_n = \frac{2}{M} \left[1 - \left(\frac{ka + 2\pi n}{k_{n_0} a} \right)^2 \right]$$

$$k_{n_0} a = k_0 a + 2\pi m n, \quad k_0 = \omega/v_{p_0}, \quad a = 2\pi/k_1$$

$$v_{p_0} = (L_0 C_0)^{-1/2}, \quad m = c'/v_{p_0}.$$

Furthermore, it has been shown [9] that such a recursion relation may be used to derive a dispersion relation (between ω and k) in the form of infinite continued fractions in the D_n 's as follows:

$$D_n = \frac{1}{D_{n-1} - \frac{1}{D_{n-2} - \frac{1}{\dots - \frac{1}{D_{n+1} - \frac{1}{D_{n-2} - \frac{1}{\dots}}}}}} = 0. \quad (4)$$

Solutions of (4) determine the relationship of $k(\omega)$ or $\omega(k)$, for specified parameters ω_1 , c' , and M , to any degree of accuracy desired. Previous analyses of this type [10], [11] have not considered interaction effects of all harmonics (n) in obtaining the propagation characteristics.

The dispersion relation has been investigated in two cases herein, outside of the sonic region, where the solutions are valid. The first case examined is that for which the pump velocity is less than the propagation velocity ($c' < v_{p_0}$). Here, all interactions take place where the frequency condition $\omega > \omega_1$ is satisfied. The results are shown in Fig. 2, for the fixed parameters $M = 0.25$ and $m = c'/v_{p_0} = 0.25$, with the plot normalized to a third parameter: $a = 2\pi/k_1$. The dispersion curve is that typical of a "stop-band" in spatially periodic structures and, indeed, the static modulation case occurs here in the limit $c' = 0$.

The region of the Brillouin diagram shown in Fig. 2 is that of the principal interaction of the fundamental wave ($n = 0$, forward group velocity) with the first harmonic ($n = -1$, backward group velocity). In the absence of interaction ($M = 0$), the two waves would be represented on the Brillouin diagram by two straight lines at $\pm 45^\circ$ (not shown) intersecting in the middle of the stop-band. The corresponding lines for any of the harmonics for this structure are described in general by

$$ka = -2\pi n \pm (k_0 a + 2\pi m n). \quad (5)$$

* Received by the PGMTT, September 20, 1961.
This work was sponsored by the A F Cambridge Res. Labs. under Contract AF 19(604)-7499.